Insight into the design and fabrication of a leaf mimicking micropump

Prashant Agrawal
Smart Materials and Surfaces Laboratory, Faculty of Engineering and Environment, Northumbria University, Newcastle upon Tyne, NE1 8ST, United Kingdom

Prasoon Kumar*
Department of Medical Devices, National Institute of Pharmaceutical Education and Research Ahmedabad, Gandhinagar, Gujarat, India
(Dated: June 19, 2019)

A micropump is the heart of any microfluidic device that finds applications in several lab-on-chip devices. Passive micropumps are highly desirable for this purpose due to their ease of integration, low energy requirements and simplistic design and operation. The design of a plant leaf serves as a natural inspiration for developing an evaporation assisted passive micropump. The presence of branching channel like venation pattern ensures water distribution to the spongy mesophyll cells increasing the surface area for evaporation. However, due to its multiscale design and complexity of the venation pattern, emulating a leaf's design is challenging. Apart from the lack of understanding of design parameters that affect fluid flow, manufacturing limitations impede the development of such bio-inspired micropumps. Inspired by the multi-scale design of the leaf, in this work we propose a passive micropump mimicking the structure of a leaf. Employing evaporation and capillary pressure as the pumping mechanism, our leaf mimicking micropump consists of a microporous membrane integrated with a branched, fractal channel network resembling a leaf's venation pattern. Our proposed fabrication methodology is simple, scalable, inexpensive and uses readily available materials. We demonstrate a significant increase in the fluid flow rate due to the addition of this branched channel network. We support our experimental observations using an analytical model, wherein we discuss the design parameters that affect the pumping rate. Correspondingly, the performance of these micropumps can be optimized based on intrinsic and extrinsic factors as per the desired applications.

I. INTRODUCTION

Micropumps form an integral part of many microfluidic systems where precise control over fluid delivery is required. Such controlled delivery is desirable in applications like advanced drug delivery systems, lab-on-chip devices and microelectronic cooling system[1–3]. Passive micropumps offer promising solutions as they can circumvent problems posed by active micropumps[4–6] such as energy consumption, actuation mechanism integration and oscillating/pulsating flows. Towards the development of such passive micropumps, tree leaves in nature have served as an inspiration for evaporation assisted passive micropumping for microfluidic applications[7].

Several studies have looked at developing artificial leaf systems focusing either on the use of novel materials[8–10] or device design to increase the surface area of evaporation[11–13]. Hydrogels have been recently proposed as a material for water storage and imbibition applications[14]. A low chemical potential of water in hydrogels imparts high mobility to water molecules, which allows for large pressure heads for wicking water[15]. Such hydrogels can be used to simultaneously function as a tree trunk (for water transportation) and as a leaf (for evaporation)[14]. Hydrogels can also be combined with microporous membranes to help control the evaporative flux based on the pore size[13]. Additional designs include mimicking the functional and structural form of leaves with slit-like micropores acting like a leaf's stomata[16]. Using thermo-responsive polymers, these slit-like pores can be actuated to emulate the closure of a leaf's stomata with variation in temperature, thereby controlling the pumping rate[17].

Although hydrogels provide high pressure heads, they are structurally weak materials, and are less suitable in applications demanding structural support and relatively large flow rates[18]. As an alternative, microporous substrates have been used to provide structural stability with a relative fabrication ease. In these substrates the capillary pressure in the pores of the substrate provides the necessary pressure head for pumping. Therefore, the flow rate primarily depends on the material and size of the pores, which also dictates the available evaporative surface area[19]. Here, the length and diameter of the channel irrigating the substrate (analogous to a tree trunk) does not alter the pressure head or pumping rate significantly[19]. However, by incorporating a multi-channel pattern that irrigates the substrate, the net evaporative flux can be significantly enhanced[20]. Here the density and shape of the pattern is crucial in lowering the flow resistance and increasing the surface area of evaporation. Previous studies have primarily used parallel arrays of rectangular channels to mimic this venation pattern as fabricating a 3D multi-scale branching channel is complex and relies on expensive lithographic processes[21]. Further, the parallel channel designs are not necessarily optimized for lowering the fluid flow resistance.

Therefore, in the present work, we propose a novel design of a passive micropump that mimics the venation pattern of a leaf using a simple, inexpensive and scalable fabrication method (depicted in Figure 1). The leaf-mimicking micropump (LMM) comprises of radially arranged, 3D, branch shaped, multi-scale microchannels (representing leaf

* prasoon.kumar@niperahm.ac.in

veins) integrated into a microporous substrate (resembling stomata and spongy mesophyll cells). We compare the evaporative flow rate obtained in the LMM with a control substrate devoid of the venation pattern. The LMM demonstrated enhanced flow rates compared to similar microporous membrane based passive micropumps. Further, we use an analytical model to validate and explain the performance of the micropumps. The model used here agrees with experiments and can serve as a guide for the design and fabrication of such bio-inspired micropumps for specific applications.

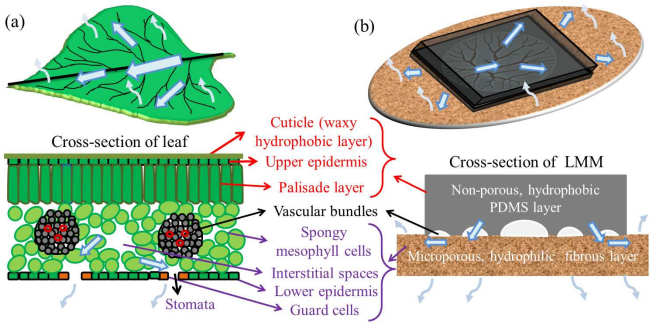

FIG. 1: Concept of a Leaf Mimicking Micropump (LMM): (a) The macro and microstructure of the leaf, (b) The analogous structure of the LMM

II. METHODS

A. Device fabrication

The fabrication process of the LMM is shown in Figure 2 (a). The fractal microchannel network was obtained using a bespoke Hele-Shaw apparatus based on Saffman-Taylor instabilities[22]. A thoroughly mixed ceramic suspension was used to create the mold for the fractal channel network[23]. The channel network obtained from the Hele-Shaw apparatus was heated over a hot plate at 120 °C for a period of 24 hours to cure and form a stable mold ready for casting. After curing PDMS (Sylgard; elastomer:curing agent weight ratio=10:1) was poured over the mold and allowed to cure over a hot plate. The cured PDMS (thickness $\approx$ 2 mm) was then peeled off to form the open fractal microchannel network (structural characterization details are provided in supplementary information). To integrate the channel network with a microporous substrate, PDMS was spin coated at 800 rpm for 2-3 minutes on a paraffin wax paper, and left at room temperature for 24 hours to cure it partially. This partially cured PDMS film is then placed on a microporous filter paper (Whatman, 90 mm diameter) which are bonded together by heating at 100 °C for 15 seconds. Thereafter, the paraffin wax paper was carefully removed and the cured fractal channel network substrate was pressed on the exposed side of the PDMS film, which is adhered to the microporous substrate on the other side. The entire device was then heated at 60 °C for about 1.5 hours to cure the PDMS film and hence, strengthen the bonding between the fractal channel substrate and the microporous filter paper. The diameter of the bonding PDMS film is such that the terminal ends of the fractal channel are in direct contact with the microporous substrate.

B. Experimental setup

The fabricated LMM was placed on a stage (as depicted in Figure 2) such that the outer part of the substrate was exposed for evaporation. The LMM was connected to one end of a PTFE tube (length 790 mm and internal diameter 2 mm) while the other end of the tube was placed in a reservoir as depicted in Figure 2 (b). Initially, the reservoir and LMM were placed at the same level from the ground. The reservoir was then slowly raised above the LMM by 2 mm to enable water to flow through the tube to the microporous substrate. The flow of water from the reservoir was continued till the entire microporous substrate was saturated. This preconditioning is necessary to avoid the effect of water absorption by the dry substrate on the measured flow rates. Next, the reservoir was lowered till the level of the LMM and left for 15 minutes to reach a steady state. In this steady state condition, the volumetric flow through the microporous substrate is equal to the evaporative flux of water from the exposed surface of the substrate. Next, an air bubble was introduced in the tube from the end placed in the reservoir. The LMM was left in an open air in clean room environment at 25°C and relative humidity of 50%. The fluid pumping velocity was measured by tracking the movement of the air bubble in the tube. To assess the pressure head generated by the LMM, the platform on which the LMM was placed was raised in steps and allowed to stabilize for 15 minutes at each step before tracking the air bubble movement. The process of raising the LMM was ceased when there was no appreciable change in the position of the air bubble. Control experiments were carried out with a device, wherein, a PTFE tube (of the same length) was connected directly to the microporous substrate without any intermediate microchannel network.

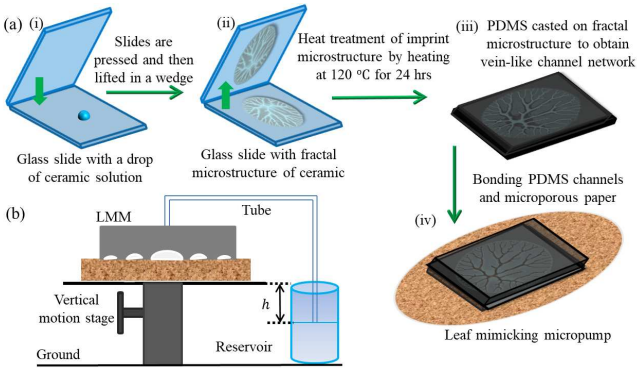

FIG. 2: (a) Fabrication procedure for the LMM, (b) Experimental setup for measuring the flow rate from the LMM at different pressure heads

III. RESULTS AND DISCUSSION

A. LMM flow characterization

The flow rates obtained from the LMM and the control device are shown in Figure 3. At zero pressure head ($h = 0\,\text{mm}$), the average liquid pumping rate ($\dot{M}_e$) of the LMM is about $0.108\,\text{mg}\,\text{s}^{-1}$, which is approximately 10 times higher than that of the control device ($\dot{M}_e \approx 0.018\,\text{mg}\,\text{s}^{-1}$). In this LMM design, the increased evaporative pumping rate is obtained by enhancing the surface area available for evaporation. The presence of the fractal channel network eases the delivery of the liquid to multiple radially distributed locations on the substrate from the liquid source (PTFE tube). These multiple irrigation points increase the net radial spread of the liquid as it imbibes into the microporous substrate. In the absence of this fractal channel network, as in the control device, the pores of the microporous substrate offer a relatively higher resistance to liquid flow for the same spreading area as in the LMM. This higher flow resistance results in a smaller radial spread of the liquid and, hence, reduced evaporative pumping rates. Therefore, the integration of the fractal channel network effectively reduces the net resistance to the liquid flow leading to a larger surface area available for evaporation.

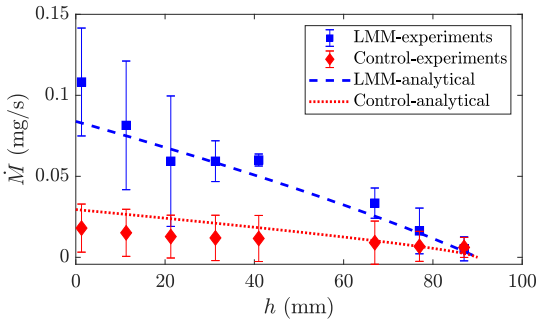

FIG. 3: Experimental results for mass flow rate against height of the LMM. The dashed line represents the trend for the LMM setup from equation 3 and the dotted line represents the trend for the control setup from equation 4.

Next, by changing the height of the LMM with respect to the reservoir, we look at the variation of the mass flow rate with pressure head. We observe that the liquid pumping rates of the LMM decline approximately 10 times faster than that in the control microporous substrate (Figure 3). As the height is increased, bubbles are observed around the terminal ends of the channel network at around 40 mm. This bubble entrainment is a limitation of the fabrication process which can be overcome by improving the contact between the terminal ends of the channel with the microporous substrate. With further increase in height these bubbles nucleate and migrate towards the tube connecting the reservoir to the LMM device. Above a height of approximately 85 mm, the capillary pressure in the substrate is unable to sustain the flow, wherein, air bubbles completely block the flow terminal ends of the channel network and prevent liquid flow.

B. Analytical model

To investigate the difference in the behavior of the LMM with the control substrate, we analytically model the evaporation rate as a function of the LMM height. At steady state, the continuous pumping is driven by evaporation from the exposed area of the microporous substrate. This flow is resisted by the gravitational pressure head introduced by raising the LMM and the viscous friction arising from the flow in the porous substrate, the fractal channel network and the tubing connecting the LMM to the liquid source. We assume that the terminal ends of the fractal channel form a continuous ring-like liquid source and adopt the model developed by Liu *et al*[24]. At steady state the flow in the porous substrate is described by:

$$P_c' = \frac{\mu \dot{m}_e R_0^2}{4K\rho H}(1 - x + x\log x). \tag{1}$$

Here, $\dot{m}_e$ is the rate of evaporation per unit area from the surface (assumed to be constant under the same atmospheric conditions and substrate type), K is the permeability of the porous substrate, H is the thickness of the porous substrate, ρ and μ are the density and the viscosity of the liquid, R_0 is the radius of the liquid source and $x = R^2/R_0^2$, where R is the radius of the wetted region. Due to the ring-like configuration of the liquid source, there will be two solutions to x corresponding to $R_{max} \subseteq R > R_0$ and $R_{min} \subseteq R < R_0$. However, considering the orientation of the substrate in the experiments (Figure 2 (b)), we consider only one solution of x for comparison with experiments: $x = R_{max}/R_0$. P_c' is the modified capillary pressure driving the imbibition, accounting for the gravitational pressure head (P_g), the viscous pressure losses in the fractal channel (P_{vf}) and the viscous pressure losses in the tube from reservoir to the leaf (P_{vt}): $P_c' = P_c - P_{vf} - P_{vt} - P_g$, where, P_c is the capillary pressure in the microporous substrate. Considering the orientation of the substrate in the experiments, the total evaporative mass flux ($\dot{M}_e$) can be written as $\dot{M}_e = \dot{m}_e \pi (R_{max}^2 - R_0^2)$. Therefore, equation 1 can be re-written as:

$$\frac{P_c - \rho g h}{c_e \dot{m}_e R_0^2} = x\log x + \left(\frac{c_v}{c_e} - 1\right)(x - 1), \tag{2}$$

where, h is the height of the micropump above the reservoir and $c_v = c_{vt} + c_{vf}$. Here, c_{vt} and c_{vf} represent the coefficient of fluid flow resistance due to viscous friction in the tube and the fractal channel, respectively. Thus c_v represents the coefficient of fluid flow resistance due to viscous friction in the macro channels, while c_e represents the resistance to flow provided by the microporous substrate. Obtaining accurate values of the flow properties of the microporous substrate is challenging as the permeability estimation is highly dependent on the environmental and setup configurations[25]. Nevertheless, we use approximate analytical values (details in supplementary information) to estimate the relative magnitude

of the coefficients. For the current LMM design we obtain $c_v/c_e \approx 1$ for the LMM and $c_v/c_e << 1$ for the control sample. Therefore, for the LMM, equation 2 can be written as:

$$\frac{P_c - \rho g h}{c_e \dot{m}_e R_0^2} = x \log x, \tag{3}$$

while for the control sample ($c_v/c_e << 1$) equation 2 can be written as

$$\frac{P_c - \rho g h}{c_e \dot{m}_e R_0^2} = x \log x - (x-1). \tag{4}$$

The above equations are solved for x, to obtain the spreading area and therefore the evaporation rate ($\dot{M}_e = \dot{m}_e \pi R_0^2 (x-1)$) against the pressure head; assuming P_c corresponds to the pressure at h_{max} =85 mm. As the values used in the analytical model are estimates, we compare the evaporation rates with experiments by adding a scaling factor (approximately 0.03). This adjustment provides information about the variation of the mass flow rate with height, as opposed to exact numeric values. As a result, we see in Figure 3 that the trends for the LMM and the control sample agree with experimental observations, which affirms the validity of the modeling procedure.

The model can also be used to optimize the design of the LMM for different gravitational pressure heads. Considering evaporation from the entire surface of the LMM, Figure 4 shows the complete solution of equation 1, (for R_{max} and R_{min}) for different source radii (R_0); the source radius here is varied by changing the number of generations of the fractal channel network. A change in the pressure head alters both the outer and inner wetting radii of the substrate, which affect the wetted area and therefore, the flow rate. At small gravitational pressure heads, the inner surface of the LMM is completely wetted ($R_{min} = 0$). However, at higher gravitational heads, the suction pressure is insufficient to wet the inner area of the substrate completely ($0 < R_{min} < R_0$), where R_{min} depends on R_0 as seen in Figure 4. The inset shows a maximum evaporative area (A_f) for all pressure heads, which is at around 3-5 generations of the fractal channel network. The model thus informs device design, where, R_{max} provides the maximum device size, while R_{min} can be reduced to optimize the wetted area.

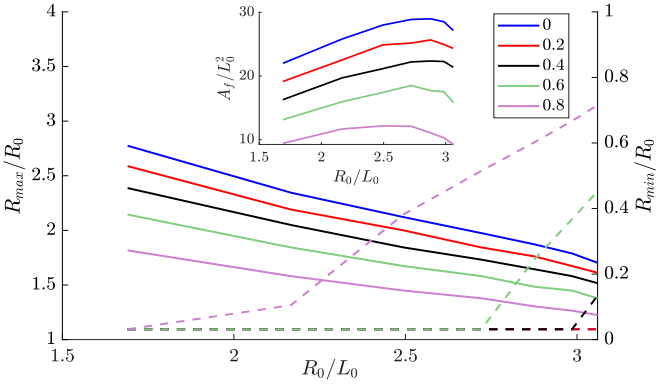

FIG. 4: Variation of the wetted area with R_0/L_0 for different gravitational pressure head ratios (h/h_{max}); L_0 is the length of the parent fractal network branch (details in supplementary information). The dashed lines represent the left y-axis (R_{max}/R_0) and the dashed lines represent the right y-axis (R_{min}/R_0). The inset shows the variation of the evaporative surface area for different pressure head ratios.

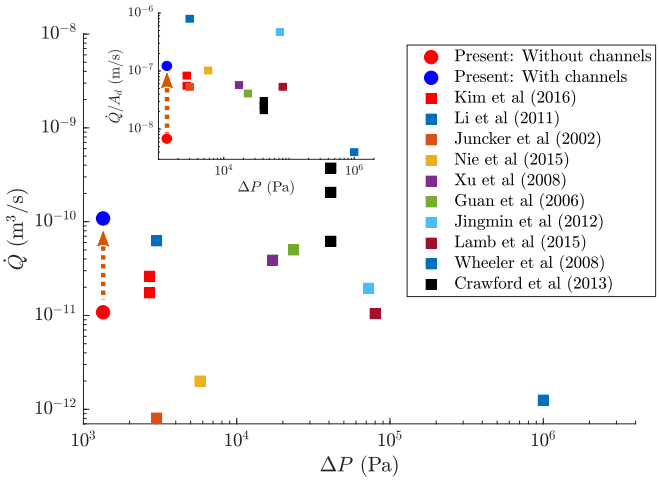

FIG. 5: Comparison of the LMM performance with previous studies. The plot compares the volumetric flow rate with a representative parameter accounting for the material properties and environmental conditions[8, 11, 13, 14, 16, 17, 19, 26–28]

C. Comparison with previous research

The evaporative capacity of any device can be broadly characterized based on two factors: material properties and device design. Using the analogy of hydraulic circuits, the volume flow rate can be written as $\dot{Q} = \Delta P / R_h$, where, ΔP is the pressure gradient (suction pressure) and R_h is the hydraulic resistance. This expression allows us to compare the performance of the LMM with previously reported passive micropumps in Figure 5. Here ΔP represents the material properties (pore size, water potential), while $\dot{Q}$ incorporates information about substrate texture and evaporative area (assuming similar environment conditions).

The flow rate obtained from the LMM is comparatively similar to that observed in some other reported passive devices, despite a relatively low suction pressure. However, Figure 5 does not present a complete and fair comparison as some of the examples use device sizes designed for specific applications and not necessarily for assessing the performance limit of their designs (apart from Crawford et al[19]). Although the inset in Figure 5 negates the influence of device size by plotting the flow rate per unit device area, the comparison does not differentiate between completely wetted and partially wetted substrates. Nevertheless, we can see that due to the addition of the venation pattern, the flow rate increases for the same suction pressure. A similar flow rate

enhancement can be obtained if such a venation pattern is included in other designs with a higher suction pressure.

IV. CONCLUSION

In this work we have demonstrated the working of a leaf inspired passive micropump. The uniqueness of the pump lies in the branched channel network that irrigates the microporous substrate to increase the evaporative surface area, which significantly enhances the pumping rate. Our manufacturing process provides a simple, inexpensive and scalable method for fabricating the a multiscale branched channel network (like veins of a leaf), and its integration with any microporous membrane. Analytical modelling of the flow suggests an ideal branching venation pattern for different pressure heads that decreases the overall hydraulic resistance to flow and maximizes the utilization of the substrate surface area during evaporation process. Threfore, our model and fabrication process can be used as a design template for developing passive micropumps using different substrates (microporous membrane or gel based) for operation in different environmental conditions.

ACKNOWLEDGMENTS

Authors would like to acknowledge IITB-Monash Research Academy and Suman Mashruwala Advanced Microengineering lab for providing funding and lab facilities to carry out experimental part of the above work.

[1] D. J. Laser and J. G. Santiago, "A review of micropumps," Journal of Micromechanics and Microengineering **14**, R35–R64 (2004).
[2] Nils Goedecke, Jan Eijkel, and Andreas Manz, "Evaporation driven pumping for chromatography application," Lab Chip **2**, 219–223 (2002).
[3] Dor Daniel, Albert Mosyak, Roza Akhvlediani, Alon Hoffman, and Gilad Yossifon, "Enhanced cooling of electronic chips using combined diamond coating and microfluidics," Phys. Rev. Applied **11**, 014047 (2019).
[4] Zihan Tan, Mingcheng Yang, and Marisol Ripoll, "Microfluidic pump driven by anisotropic phoresis," Phys. Rev. Applied **11**, 054004 (2019).
[5] A. J. Conde, A. Bianchetti, F. E. Veiras, A. Federico, J. M. Cabaleiro, M. Dufva, R. E. Madrid, and L. Fraigi, "A polymer chip-integrable piezoelectric micropump with low backpressure dependence," RSC Adv. **5**, 49996–50000 (2015).
[6] Shawn Litster, Matthew E. Suss, and Juan G. Santiago, "A two-liquid electroosmotic pump using low applied voltage and power," Sensors and Actuators A: Physical **163**, 311 – 314 (2010).
[7] Andrew J. McElrone, Brendan Choat, Greg A. Gambetta, and Craig R. Brodersen, "Water uptake and transport in vascular plants," Nature Education Knowledge **4**, 6 (2013).
[8] Marilla Lamb, George W. Koch, Eric R. Morgan, and Michael W. Shafer, "A microfluidic pump/valve inspired by xylem embolism and transpiration in plants," in *Proc. SPIE, Bioinspiration, Biomimetics, and Bioreplication*, Vol. 9429 (2015).
[9] Minki Lee, Hosub Lim, and Jinkee Lee, "Fabrication of Artificial Leaf to Develop Fluid Pump Driven by Surface Tension and Evaporation," Scientific Reports **7**, 14735 (2017).
[10] Tingjiao Zhou, Jinbin Yang, Deyong Zhu, Jieyao Zheng, Stephan Handschuh-Wang, Xiaohu Zhou, Junmin Zhang, Yizhen Liu, Zhou Liu, Chuanxin He, and Xuechang Zhou, "Hydrophilic sponges for leaf-inspired continuous pumping of liquids," Advanced Science **4**, 1700028 (2017).
[11] David Juncker, Heinz Schmid, Ute Drechsler, Heiko Wolf, Marc Wolf, Bruno Michel, Nico de Rooij, and Emmanuel Delamarche, "Autonomous microfluidic capillary system," Analytical Chemistry **74**, 6139–6144 (2002).
[12] Xiao Wang, Joshua A Hagen, and Ian Papautsky, "Paper pump for passive and programmable transport," Biomicrofluidics **7**, 14107 (2013).
[13] Li Jingmin, Liu Chong, Xu Zheng, Zhang Kaiping, Ke Xue, and Wang Liding, "A microfluidic pump/valve inspired by xylem embolism and transpiration in plants," PLOS ONE **7**, 1–5 (2012).
[14] Tobias D. Wheeler and Abraham D. Stroock, "The transpiration of water at negative pressures in a synthetic tree," Nature **455**, 208–212 (2008).
[15] Vladimir M. Gunko, Irina N. Savina, and Sergey V. Mikhalovsky, "Properties of water bound in hydrogels," Gels **3**, 37 (2017).
[16] Jing Min Li, Chong Liu, Kai Ping Zhang, Xue Ke, Zheng Xu, Chun Yu Li, and Li Ding Wang, "A micropump based on water potential difference in plants," Microfluidics and Nanofluidics **11**, 717–724 (2011).
[17] Hyejeong Kim, Kiwoong Kim, and Sang Joon Lee, "Compact and thermosensitive nature-inspired micropump," Scientific Reports **6**, 36085 (2016).
[18] El-Sherbiny Ibrahim M and Magdi H Yacoub, "Hydrogel scaffolds for tissue engineering: Progress and challenges," Global cardiology science & practice **2013**, 316342 (2013).
[19] Robert Crawford, Thomas E. Murphy, Alexandre K. da Silva, and Halil Berberoglu, "Experimental characterization of the effects of geometric parameters on evaporative pumping," Experimental Thermal and Fluid Science **51**, 183 – 188 (2013).
[20] X. Noblin, L. Mahadevan, I. A. Coomaraswamy, D. A. Weitz, N. M. Holbrook, and M. A. Zwieniecki, "Optimal vein density in artificial and real leaves," Proceedings of the National Academy of Sciences **105**, 9140–9144 (2008).
[21] Yongping Chen and Ping Cheng, "An experimental investigation on the thermal efficiency of fractal tree-like microchannel nets," International Communications in Heat and Mass Transfer **32**, 931 – 938 (2005).

[22] Tanveer ul Islam and Prasanna S. Gandhi, "Fabrication of multscale fractal-like structures by controlling fluid interface instability," Scientific Reports **6**, 37187 (2016).

[23] Chandrashekhar V. Adake, Parag Bhargava, and Prasanna S. Gandhi, "Effect of surfactant on dispersion of alumina in photopolymerizable monomers and their uv curing behavior for microstereolithography," Ceramics International **41**, 5301 – 5308 (2015).

[24] Mingchao Liu, Jian Wu, Yixiang Gan, Dorian A. H. Hanaor, and C. Q. Chen, "Evaporation limited radial capillary penetration in porous media," Langmuir **32**, 9899–9904 (2016).

[25] R. Arbter, J.M. Beraud, C. Binetruy, L. Bizet, J. Brard, S. Comas-Cardona, C. Demaria, A. Endruweit, P. Ermanni, F. Gommer, S. Hasanovic, P. Henrat, F. Klunker, B. Laine, S. Lavanchy, S.V. Lomov, A. Long, V. Michaud, G. Morren, E. Ruiz, H. Sol, F. Trochu, B. Verleye, M. Wietgrefe, W. Wu, and G. Ziegmann, "Experimental determination of the permeability of textiles: A benchmark exercise," Composites Part A: Applied Science and Manufacturing **42**, 1157 – 1168 (2011).

[26] Chuan Nie, Arjan J. H. Frijns, Rajesh Mandamparambil, and Jaap M. J. den Toonder, "A microfluidic device based on an evaporation-driven micropump," Biomedical Microdevices **17**, 47 (2015).

[27] Zhang-Run Xu, Chong-Hui Zhong, Yan-Xia Guan, Xu-Wei Chen, Jian-Hua Wang, and Zhao-Lun Fang, "A microfluidic flow injection system for dna assay with fluids driven by an on-chip integrated pump based on capillary and evaporation effects," Lab Chip **8**, 1658–1663 (2008).

[28] Yan-Xia Guan, Zhang-Run Xu, Jing Dai, and Zhao-Lun Fang, "The use of a micropump based on capillary and evaporation effects in a microfluidic flow injection chemiluminescence system," Talanta **68**, 1384 – 1389 (2006).